The Astrophysical Journal Letters, 947:L31 (11pp), 2023 April 20 https://doi.org/10.3847/2041-8213/acc9b5

DESI Survey Validation Spectra Reveal an Increasing Fraction of Recently Quenched Galaxies at $z \sim 1$

David J. Setton[1], Biprateep Dey[1], Gourav Khullar[1], Rachel Bezanson[1], Jeffrey A. Newman[1], Jessica N. Aguilar[2], Steven Ahlen[3], Brett H. Andrews[1], David Brooks[4], Axel de la Macorra[5], Arjun Dey[6], Sarah Eftekharzadeh[7], Andreu Font-Ribera[8], Satya Gontcho A Gontcho[2], Anthony Kremin[2], Stephanie Juneau[6], Martin Landriau[2], Aaron Meisner[6], Ramon Miquel[8,9], John Moustakas[10], Alan Pearl[1], Francisco Prada[11], Gregory Tarlé[12], Małgorzata Siudek[13,14], Benjamin Alan Weaver[6], Zhimin Zhou[15], and Hu Zou[15]
[1] Department of Physics and Astronomy and PITT PACC, University of Pittsburgh, Pittsburgh, PA 15260, USA; davidsetton@pitt.edu
[2] Lawrence Berkeley National Laboratory, 1 Cyclotron Road, Berkeley, CA 94720, USA
[3] Boston University, 590 Commonwealth Avenue, Boston, MA 02215, USA
[4] Department of Physics & Astronomy, University College London, Gower Street, London, WC1E 6BT, UK
[5] Instituto de Física, Universidad Nacional Autónoma de México, Cd. de México C.P. 04510, Mexico
[6] NSF's NOIRLab, 950 North Cherry Avenue, Tucson, AZ 85719, USA
[7] SOFIA Science Center, NASA Ames Research Center, Moffett Field, CA 94035, USA
[8] Institut de Física d'Altes Energies (IFAE), The Barcelona Institute of Science and Technology, Campus UAB, E-08193 Bellaterra Barcelona, Spain
[9] Institució Catalana de Recerca i Estudis Avançats, Passeig de Lluís Companys, 23, E-08010 Barcelona, Spain
[10] Department of Physics and Astronomy, Siena College, 515 Loudon Road, Loudonville, NY 12211, USA
[11] Instituto de Astrofísica de Andalucía (CSIC), Glorieta de la Astronomía, s/n, E-18008 Granada, Spain
[12] University of Michigan, Ann Arbor, MI 48109, USA
[13] Institute of Space Sciences (ICE, CSIC), Campus UAB, Carrer de Magrans, E-08193 Barcelona, Spain
[14] Institut de Física d'Altes Energies (IFAE), The Barcelona Institute of Science and Technology, E-08193 Bellaterra (Barcelona), Spain
[15] National Astronomical Observatories, Chinese Academy of Sciences, A20 Datun Road, Chaoyang District, Beijing, 100012, People's Republic of China
Received 2022 December 9; revised 2023 March 3; accepted 2023 April 1; published 2023 April 25

Abstract

We utilize ∼17,000 bright luminous red galaxies (LRGs) from the novel Dark Energy Spectroscopic Instrument Survey Validation spectroscopic sample, leveraging its deep (∼2.5 hr galaxy^{-1} exposure time) spectra to characterize the contribution of recently quenched galaxies to the massive galaxy population at $0.4 < z < 1.3$. We use `Prospector` to infer nonparametric star formation histories and identify a significant population of recently quenched galaxies that have joined the quiescent population within the past ∼1 Gyr. The highest-redshift subset (277 at $z > 1$) of our sample of recently quenched galaxies represents the largest spectroscopic sample of post-starburst galaxies at that epoch. At $0.4 < z < 0.8$, we measure the number density of quiescent LRGs, finding that recently quenched galaxies constitute a growing fraction of the massive galaxy population with increasing look-back time. Finally, we quantify the importance of this population among massive ($\log(M_\star/M_\odot) > 11.2$) LRGs by measuring the fraction of stellar mass each galaxy formed in the gigayear before observation, $f_{1\,\mathrm{Gyr}}$. Although galaxies with $f_{1\,\mathrm{Gyr}} > 0.1$ are rare at $z \sim 0.4$ ($\lesssim$0.5% of the population), by $z \sim 0.8$, they constitute ∼3% of massive galaxies. Relaxing this threshold, we find that galaxies with $f_{1\,\mathrm{Gyr}} > 5\%$ constitute ∼10% of the massive galaxy population at $z \sim 0.8$. We also identify a small but significant sample of galaxies at $z = 1.1$–1.3 that formed with $f_{1\,\mathrm{Gyr}} > 50\%$, implying that they may be analogs to high-redshift quiescent galaxies that formed on similar timescales. Future analysis of this unprecedented sample promises to illuminate the physical mechanisms that drive the quenching of massive galaxies after cosmic noon.

Unified Astronomy Thesaurus concepts: Post-starburst galaxies (2176); Galaxies (573); E+A galaxies (424); Galaxy quenching (2040); Quenched galaxies (2016); Galaxy spectroscopy (2171); Redshift surveys (1378)

1. Introduction

In the local universe, the vast majority of massive ($\log(M_\star/M_\odot) \gtrsim 11$) galaxies are completely quiescent and have been so for 5–10 Gyr (e.g., Muzzin et al. 2013; Donnari et al. 2019; Leja et al. 2022; Weaver et al. 2022). There is a growing consensus that two distinct pathways to quiescence are at play, with a rapid path dominating the buildup of quiescent galaxies at high redshifts and a slower channel that populates the "green valley" at low redshift (e.g., Schawinski et al. 2014; Maltby et al. 2018; Wu et al. 2018; Belli et al. 2019; Suess et al. 2021). While the observational evidence for more rapid early star formation in the most massive systems at early times is strong (e.g., "downsizing" trends observed in Juneau et al. 2005), the precise details of how the quiescent population grows from the rapid quenching pathway as a function of cosmic time remain very uncertain. Some studies have characterized the rates of rapid quenching as a function of cosmic time using either photometric (Whitaker et al. 2012; Wild et al. 2016; Belli et al. 2019; Park et al. 2022) or shallow spectroscopic (Rowlands et al. 2018) samples and found that recently quenched galaxies, sometimes known as post-starburst galaxies, stopped contributing significantly to the quiescent population by $z \gtrsim 0.5$. However, photometric studies yield weak constraints on timescales and star formation histories. Thus, our picture of precisely when galaxies shut off their star formation and the

contribution of late-time star formation remain poorly constrained.

Ideally, one would study the assembly of the red sequence by modeling the star formation histories of complete samples of massive galaxies and studying how the incidence and characteristics of the population vary as a function of cosmic time. An immense amount of work has been done over the past several decades to study the star formation histories of quiescent systems across cosmic time using photometric and spectroscopic data (e.g., Tinsley & Gunn 1976; Dressler et al. 2004, 2016; Daddi et al. 2005; Gallazzi et al. 2005, 2014; Pacifici et al. 2016; Belli et al. 2019; Carnall et al. 2019; Tacchella et al. 2022). However, measuring the high-order moments of a star formation history, such as timescales and burst fractions, requires high signal-to-noise ratio continuum spectroscopy (Suess et al. 2022b). The limiting factor in performing such modeling has been the availability of sufficiently deep spectra beyond $z \gtrsim 0.5$. The largest existing spectroscopic samples have not prioritized observing the gamut of quiescent galaxies; the Sloan Digital Sky Survey (SDSS) luminous red galaxy (LRG; Eisenstein et al. 2001) and BOSS (Dawson et al. 2013) surveys targeted the reddest quiescent galaxies, prioritizing pure, uniform samples at the expense of younger, bluer galaxies with targeting that steeply drops off at $z \sim 0.5$, where the post-starburst population beings to emerge (Wild et al. 2016; Belli et al. 2019). In contrast, the EBOSS (Dawson et al. 2016) survey poorly sampled the quiescent population in favor of more accessible emission line sources. Deeper, more targeted surveys such as LEGA-C (Wu et al. 2018; van der Wel et al. 2021), Carnegie–Spitzer–IMACS (Dressler et al. 2016), and VANDELS (McLure et al. 2018; Carnall et al. 2019) have identified samples of ∼thousands of massive quiescent galaxies at $z \gtrsim 0.5$, requiring significant investments on deep fields to reveal spectroscopic information for small samples.

The next generation of large spectroscopic surveys will revolutionize the availability of continuum spectroscopy of massive galaxies. Here we utilize the Dark Energy Spectroscopic Instrument (DESI), a robotic, fiber-fed, highly multiplexed spectroscopic surveyor that operates on the Mayall 4 m telescope at Kitt Peak National Observatory (DESI Collaboration et al. 2016a). DESI, which can obtain simultaneous spectra of almost 5000 objects over an ∼3° field (DESI Collaboration et al. 2016b; Silber et al. 2023; T. Miller et al. 2023, in preparation), is currently over a year into a 5 yr survey of approximately one-third of the sky (DESI Collaboration et al. 2016a) and has already observed more galaxies than the entire SDSS. The DESI LRG target selection is broader in both color and faintness relative to surveys like BOSS, and as a result, it is complete to a higher redshift ($z \sim 0.8$) and observes the Balmer break out to $z \sim 1.3$ (Zhou et al. 2023). Here we show that even the relatively small (∼20,000 galaxies) but deep Survey Validation (SV) sample of LRGs within the DESI survey can be leveraged to identify new and exciting samples of recently quenched galaxies that push well beyond what previous surveys have been capable of.

In this letter, we infer the nonparametric star formation histories of LRGs in the DESI SV sample (DESI Collaboration et al. 2023, in preparation) and use them to study the growth of the red sequence from recently quenched galaxies. In Section 2, we describe the parent sample and demonstrate the use of nonparametric star formation histories to fit the spectrophotometric data with `Prospector` (Johnson & Leja 2017; Leja et al. 2017; Johnson et al. 2021). In Section 3, we use the results of this fitting to identify recently quenched galaxies and characterize their evolving number densities as a function of cosmic time. Finally, in Section 4, we discuss the implications of these findings for our understanding of the physical mechanisms that are driving the production of massive quiescent galaxies through the rapid quenching channel.

Throughout this letter, we compare our own selection of "recently quenched galaxies" to literature samples and selection criteria for post-starburst galaxies. We note that many of these post-starburst selections do not explicitly require a burst of star formation, as any dramatic truncation in star formation can produce an A star–dominated spectral energy distribution (SED). We assume a concordance ΛCDM cosmology with $\Omega_\Lambda = 0.7$, $\Omega_m = 0.3$, and $H_0 = 70$ km s^{-1} Mpc^{-1} and quote AB magnitudes.

2. Data

2.1. The DESI LRG SV Sample

In order to characterize the growth of the population of quiescent galaxies at intermediate redshifts, this work relies on the large program of deep spectra that were taken as a part of the DESI SV LRG sample (Zhou et al. 2020, 2023; DESI Collaboration et al. 2023, in preparation). The primary objective of DESI is to determine the nature of dark energy with precise cosmological measurements (Levi et al. 2013), but the wealth of spectroscopy provides an excellent sample for studies of galaxy evolution. The data volume of DESI requires multiple supporting software pipelines and products used in this work. Target selection and photometry, which included forward modeling of the differential effect of the point-spread function across bands, was performed on imaging from the DESI Legacy Surveys (Zou et al. 2017; Dey et al. 2019; D. Schlegel et al. 2023, in preparation). Fiber assignments, tiling, and target selection were performed with the algorithms outlined in A. Raichoor et al. (2023, in preparation), E. Schlafly et al. (2023, in preparation), and A. Myers et al. (2023, in preparation), respectively. All redshifts were determined with the `Redrock` pipeline (S. Bailey et al. 2023, in preparation). All spectroscopy was reduced using the "Fuji" internal spectroscopic data release, which will be identical to the DESI Early Data Release (Guy et al. 2023; tentatively expected in early 2023).

There are two primary reasons for the choice to utilize the SV sample. First, the SV selection is more inclusive than subsequent SV samples and the main DESI sample (see Appendix A in Zhou et al. 2023). While this was intended as a test of the redshift recovery so that targeting could be refined from the main survey, these expanded color cuts mitigate potential bias against observing young, recently quenched LRGs. Second, the SV observations were an order of magnitude deeper than the observations for the main survey, with ∼2.5 hr of integration per spectrum, resulting in the high signal-to-noise ratio measurements of the continuum. While the SV sample included fainter targets, we restrict this study to the brightest SV LRGs with an observed fiber z magnitude $z_{\rm fiber} < 21.6$ cut similar to the one that is used in the full LRG sample.

We select all tiles that were observed under the dark time observing conditions in SV. We then select all galaxies that meet the LRG SV cuts outlined in Zhou et al. (2023) with an additional $z_{\rm fiber} < 21.6$ mag constraint, a cut at $z > 0.4$ (above which the SV LRG sample begins to be mass complete), and a cut at $z < 1.3$ (at which point the age-sensitive H_δ absorption feature is no longer covered by DESI spectroscopy). We remove galaxies with poor redshift measurements by applying a cut of ZWARN == 0 to the DESI catalog. We then remove the 580/17,797 galaxies that did not reach the target depth (exposure time $t_{\rm exp} > 1$ hr). The median exposure time of this final sample is 2.4 hr, with 16th and 84th percentile exposure times of 1.5 and 4.1 hr, respectively. This selection results in a total sample of 17,217 galaxies.

2.2. Inferring Star Formation Histories with Prospector

We model the DESI spectra and photometry using nonparametric star formation histories with the SED fitting code Prospector (Johnson & Leja 2017; Leja et al. 2017; Johnson et al. 2021) to infer the detailed stellar populations of the sample. Nonparametric star formation histories are particularly useful for fitting post-starburst galaxies because they do not impose an analytic form on the shape of the star formation history, which allows for multiple rises and falls over the course of a galaxy's lifetime. We adopt a flexible bin model that is optimized to model recently quenching galaxies (Suess et al. 2022b). The model utilizes three fixed time bins at early times ($t_{\rm look\text{-}back} > 2$ Gyr), five flexible bins that each form the same amount of total stellar mass (allowing for greater resolution near periods of intense star formation), and a final flexible bin that allows a galaxy to remain quenched after star formation is finished. This scheme was extensively tested and is well designed to recover quenching timescales and burst mass fractions (Suess et al. 2022a, 2022b).

We use the dynesty dynamic nested sampling package (Speagle 2020), the Flexible Stellar Population Synthesis stellar population synthesis models (Conroy et al. 2009; Conroy & Gunn 2010), the MILES spectral library (Sánchez-Blázquez et al. 2006; Falcón-Barroso et al. 2011), and the MIST isochrones (Choi et al. 2016; Dotter 2016). We assume a Chabrier (2003) initial mass function and fix the model redshift to the spectroscopic redshift. In contrast with the Suess et al. (2022a) prescription for fitting post-starburst galaxies, we elect to fit nebular emission nonphysically by marginalizing over Gaussian lines at the locations of emission features in the spectrum. The massive LRG sample likely hosts many active galactic nuclei (AGN), which can contribute strongly to a galaxy's emission line strength (especially the recently quenched galaxies; e.g., Greene et al. 2020). Additionally, the LRG selection allows for the targeting of a small fraction of dusty star-forming galaxies with strong emission lines; we want to be completely agnostic to the source of emission when fitting star formation histories to these galaxies. This procedure subtracts out the emission from the spectrum at each step in the fitting before calculating the likelihood, which allows the fits to utilize continuum information (e.g., Hβ absorption) despite the existence of emission that our models do not generate using information about the current star formation rate (SFR).

We use the mass–metallicity prior described in Leja et al. (2019). We utilize the PolySpecModel procedure, which accounts for deviations between the shape of the photometry and the spectrum by dividing out a polynomial from the observed and model spectra during fitting using a Prospecter-default 12th-order Chebyshev polynomial. We assume the Kriek & Conroy (2013) dust law with a free A_v and dust index. Additionally, following Wild et al. (2020), we assume that the attenuation is doubled around young ($<10^7$ yr) stars. We fix the shape of the IR SED following the Draine et al. (2007) dust emission templates, with $U_{\rm min} = 1.0$, $\gamma_e = 0.01$, and $q_{\rm PAH} = 2.0$. Finally, we include both a spectroscopic jitter term to account for the possibility of underestimated noise and the Prospector pixel outlier model. We center priors on the star formation history such that they follow the predicted star formation history of a massive quiescent galaxy from the UNIVERSEMACHINE catalog (Behroozi et al. 2019); this weakly prefers solutions with early-time star formation in the star formation histories we fit to ensure that outshining of a young stellar population is treated conservatively. The fidelity of this star formation history at recovering mock parameters is illustrated in Suess et al. (2022b). Of principal importance to this work, the burst fraction is well recovered when <50% of a galaxy's stellar mass is formed in a burst. For greater burst fractions, outshining by the young stellar population becomes so dominant that the relative strength of the oldest stellar population cannot be constrained by the existing data, and as such, our conservative prior drives the fits to a higher burst fraction solution than the inputs. Thus, burst fractions measured in this work to be $\gtrsim$50% can be thought of as strong lower limits.

We fit all 17,217 galaxies in the DESI SV LRG sample ($z_{\rm fiber} < 21.6$) with this procedure, providing the Milky Way extinction-corrected $g/r/z/W1/W2$ photometry (using the extinction maps from Schlegel et al. 1998) and the galaxy spectrum. The scaling of the SED being fit is set by the photometry that captures all galaxy light, rather than just the light in the fiber. We expect the total fraction of galaxy light contained in the fiber to vary as a function of redshift but to always be $\gtrsim$50% of the total light, as the fiber size is 0.″75 in radius (4 kpc at $z = 0.4$, 6.5 kpc at $z = 1.3$). Our fits are constrained by the SED shape of the photometry, and the polynomial correction to the spectrum will account for any color gradients, though we expect those to be minimal given that the spectrum should be representative of the majority of the galaxy light for most of the sample. Because the signal in the redshift range of interest is concentrated at the red end of the spectrograph, we elect to only fit the spectra from the R and Z arms of the spectrograph (5800 Å $< \lambda_{\rm obs} <$ 9824 Å) to save on computation time and avoid any issues with the flux calibration at the fainter end of the spectra. In this wavelength range, the resolution R ($\lambda/\Delta\lambda$) ranges from ∼3200 to 5100. While the 1.″5 (∼8 kpc at $z = 0.4$, ∼13 kpc at $z = 1.3$) diameter aperture of the DESI fiber is large enough to capture the majority of galaxy light at the highest-redshift end of our sample, we do note that our modeling approach assumes a lack of color gradients in the galaxies and that the light represented in the spectrum is identical to that of the photometry, which models all galaxy light. Fits failed to converge for 52/17,217 galaxies (0.3% of the total sample). Visual inspection of the spectra of these failed fits suggests that they broadly fall into four categories: extremely low signal-to-noise ratio galaxies, spectra with large masked regions, galaxies with incorrect redshift assignments, and broad-line AGN/QSOs (which our models are not equipped to characterize). As such, we omit the

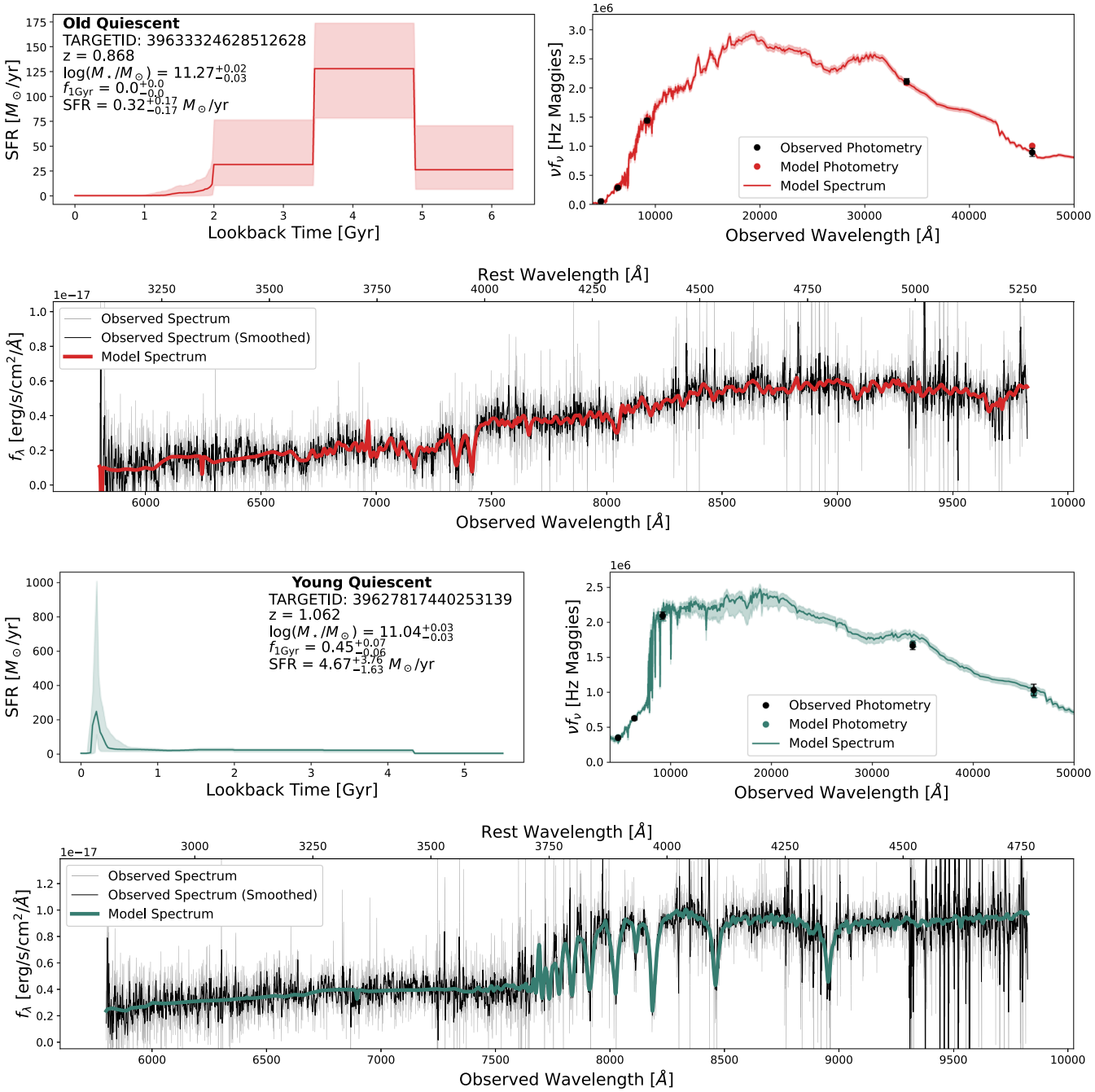

Figure 1. Example old (top; TARGETID = 3963332462851262) and recently quenched (bottom; TARGETID = 39627817440253139) galaxies from the DESI SV LRG sample with `Prospector` fits using the star formation history model from Suess et al. (2022b). For each galaxy, we show the median and 68% confidence interval star formation history(top left) with selected galaxy properties. We also show the best-fitting models (color) to the observed photometry ($g/r/z/W1/W2$; black) in the top right panels. Finally, we show the DESI spectrum (observed, gray; 5 pixel boxcar smoothed, black) along with the best-fitting model (color; bottom). From this modeling, we identify quiescent LRGs and infer the dominance of recent star formation and the timescale of quenching.

unmodeled galaxies and perform all analysis on the 17,703 successfully fit galaxies.

Example fits to quiescent (top; red) and recently quenched (bottom; green) galaxies are shown in Figure 1. The quiescent galaxy that is representative of the majority of the DESI LRG sample is fit entirely with early star formation, consistent with a very old stellar population, and as such, all of the mass was formed in the three fixed-width early-time bins. In contrast, the recently quenched galaxy is clearly fit with a post-starburst SED shape with strong Balmer absorption features and a characteristic lack of emission line infill. This indicates that the post-starburst galaxy has quenched after a period of intense star formation, and the star formation history reflects this. We infer that the galaxy began rapidly forming stars ∼500 Myr before observation and quenched ∼150 Myr ago.

From the posteriors on the star formation histories, we derive a number of model parameters, many of which we directly use to select and characterize the properties of recently quenched galaxies. Stellar masses are calculated accounting for mass loss and have typical 1σ uncertainties of 0.025 dex, and rest absolute magnitudes are calculated directly from the spectra generated from the posterior. We measure the SFR in all

Table 1
Selected Fit Quantities and Errors

z	$\log(M_\star/M_\odot)$	SFR ($M_\odot$ yr^{-1})	ΔSFR	$f_{1\ \mathrm{Gyr}}$
0.5568	$11.23^{+0.01}_{-0.01}$	$2.31^{+0.47}_{-0.35}$	$-1.16^{+0.08}_{-0.07}$	$0.11^{+0.01}_{-0.01}$
0.6701	$11.22^{+0.01}_{-0.01}$	$1.17^{+0.14}_{-0.14}$	$-1.52^{+0.05}_{-0.06}$	$0.0^{+0.0}_{-0.0}$
0.8976	$11.23^{+0.02}_{-0.1}$	$0.92^{+0.84}_{-0.31}$	$-1.76^{+0.39}_{-0.18}$	$0.0^{+0.07}_{-0.0}$
0.5396	$11.36^{+0.01}_{-0.01}$	$2.98^{+0.4}_{-0.34}$	$-1.16^{+0.06}_{-0.06}$	$0.05^{+0.01}_{-0.02}$
0.4364	$11.12^{+0.01}_{-0.01}$	$2.85^{+0.27}_{-0.24}$	$-0.9^{+0.05}_{-0.04}$	$0.01^{+0.0}_{-0.0}$
0.8807	$11.34^{+0.03}_{-0.03}$	$0.08^{+0.28}_{-0.08}$	$-2.86^{+0.62}_{-1.51}$	$0.0^{+0.0}_{-0.0}$
0.6999	$10.8^{+0.03}_{-0.04}$	$19.39^{+2.56}_{-2.4}$	$0.08^{+0.07}_{-0.09}$	$0.22^{+0.05}_{-0.04}$
0.5415	$11.11^{+0.04}_{-0.03}$	$0.09^{+0.05}_{-0.04}$	$-2.45^{+0.19}_{-0.28}$	$0.01^{+0.01}_{-0.0}$
0.5166	$11.2^{+0.02}_{-0.03}$	$21.25^{+2.17}_{-3.02}$	$-0.15^{+0.06}_{-0.08}$	$0.1^{+0.02}_{-0.02}$
1.0623	$11.04^{+0.03}_{-0.03}$	$4.67^{+3.76}_{-1.63}$	$-0.94^{+0.26}_{-0.18}$	$0.45^{+0.07}_{-0.06}$

Note. Selected median and 68% confidence values of relevant parameters derived from the posteriors of the `Prospector` fits to DESI SV LRGs for a random sample of galaxies.

galaxies as the SFR in the closest bin to the epoch of observation in the nonparametric star formation history. Above $\sim$1 $M_\odot$ yr^{-1}, these SFRs have been shown to reliably recover the instantaneous SFR of mock galaxies, and our measurements have typical uncertainties of $\sim$15%. Below this, they are effectively upper limits (Suess et al. 2022b). Additionally, we quantify the offset from the star-forming sequence, ΔSFR, as

$$\Delta\mathrm{SFR} = \log(\mathrm{SFR}) - \log(\mathrm{SFR}_{\mathrm{SFS}}(z)), \quad (1)$$

where $\mathrm{SFR}_{\mathrm{SFS}}(z)$ is the inferred SFR from the star-forming sequence at the observed redshift of the galaxy defined in Leja et al. (2022), which is also measured using `Prospector` SED fits. We set a fiducial threshold for quiescence at $\Delta\mathrm{SFR} = -0.6$, $\sim 2\sigma$ below the main sequence at a given redshift. Near the fiducial value, the typical uncertainty in ΔSFR is $\sim$0.1 dex. As with the SFR, this value is significantly more uncertain for measured values. Finally, we measure the fraction of the total stellar mass formed in the gigayear before observation, $f_{1\ \mathrm{Gyr}}$. Galaxies with small $f_{1\ \mathrm{Gyr}}$ are very well constrained to be small, and for galaxies that formed 10%–70% of their stellar mass in the past gigayear, typical uncertainties are 15%–30%. A sample of constraints on the parameters is shown in Table 1.

We show some of the observed and derived characteristics of the full LRG sample as red contours in Figure 2. In the left panel, we show the stellar mass versus the rest-frame absolute magnitude, M_z, illustrating the tight correlation between the two parameters. We additionally show lines that correspond to the cuts we make in the two parameters to construct the volume-limited samples described in Section 2.3. In the middle panel, we show the SFR versus the stellar mass along with the "star-forming sequence" at $z = 0.7$ with 0.3 dex scatter from Leja et al. (2022) to illustrate that the sample is largely quiescent. Finally, we show the sample in the recently quenched selection plane of $f_{1\ \mathrm{Gyr}}$ versus ΔSFR discussed in Section 3.1 with our fiducial cuts to select recently quenched galaxies. In all three panels, we show the fiducial sample of recently quenched galaxies as green points.

2.3. Selecting Volume-limited Samples

Because the choices made in spectroscopic targeting significantly impact the observed sample, it is necessary to select a volume-limited sample to fairly compare galaxies across redshift bins. This is especially true because the $z_{\mathrm{fiber}} < 21.6$ cut in observed magnitude would observe a faint galaxy at low redshift but not high redshift. We use the fits to the spectrophotometric data to select samples that we can use to infer number densities. Throughout this letter, we utilize three relevant samples—the full LRG sample, the rest absolute Z-magnitude-selected "magnitude-limited" sample, and the "mass-complete" sample—to select recently quenched galaxies.

2.3.1. The Magnitude-limited Sample

By virtue of being the youngest and brightest galaxies in any given quiescent sample, recently quenched galaxies have the lowest $M_\star/L$ ratios at fixed stellar mass and therefore are relatively bright compared to the majority of LRGs. As such, in order to get large, complete samples of recently quenched galaxies to study as a function of redshift, a luminosity cut will maximize the sample size. We define a magnitude-limited sample with rest-frame $M_z < -23.2$, at which the entirety of the reddest (in rest $g - z$ color, which should map to the highest $M_\star/L$ ratios) 2.5% of the LRG sample is selected at $z = 0.8$. This selection results in the largest volume-limited sample we can obtain where we expect to have observed all bright recently quenched galaxies in DESI out to $z \sim 0.8$, yielding a total of 8683 galaxies.

2.3.2. The Mass-complete Sample

While a magnitude-limited sample selects the bulk of the recently quenched galaxies in the SV sample, in order to characterize the growth of the recently quenched population relative to the fainter (at fixed stellar mass) old quiescent population, we instead require a mass-complete sample. In the redshift range $0.4 < z < 0.8$, the DESI LRG targeting only selects a sample that is $\gtrsim$80% mass complete for very massive galaxies ($\log(M_\star/M_\odot) \gtrsim 11.2$; accounting for systematic differences between the stellar masses we measure and those in Zhou et al. 2023). As such, in situations where we wish to compare to the quiescent population as a whole, we elect to use only galaxies above this stellar mass, regardless of their rest-frame M_z. This sample is significantly smaller than the magnitude-limited sample, with only 5375 galaxies above the stellar mass cut at $z < 0.8$.

We show the cuts in rest-frame M_z and stellar mass that result in the two subsamples in Figure 2(a), illustrating that the stellar mass cut is significantly more restrictive than the magnitude cut, which lets through recently quenched galaxies at masses as low as $10^{10.8}$ $M_\odot$. At fixed stellar mass, the fiducial recently quenched sample (see Section 3.1) is significantly brighter than a typical LRG (red contours), and we therefore maximize our ability to constrain the number density of recently quenched galaxies as a population by instituting a cut on the absolute magnitude.

3. Analysis

3.1. Selecting Recently Quenched Galaxies

There are a number of ways of selecting recently quenched/post-starburst galaxies, all of which share the common goal of selecting galaxies that recently quenched after a period of significant star formation (French 2021). Historically, these galaxies have been selected using a combination of emission

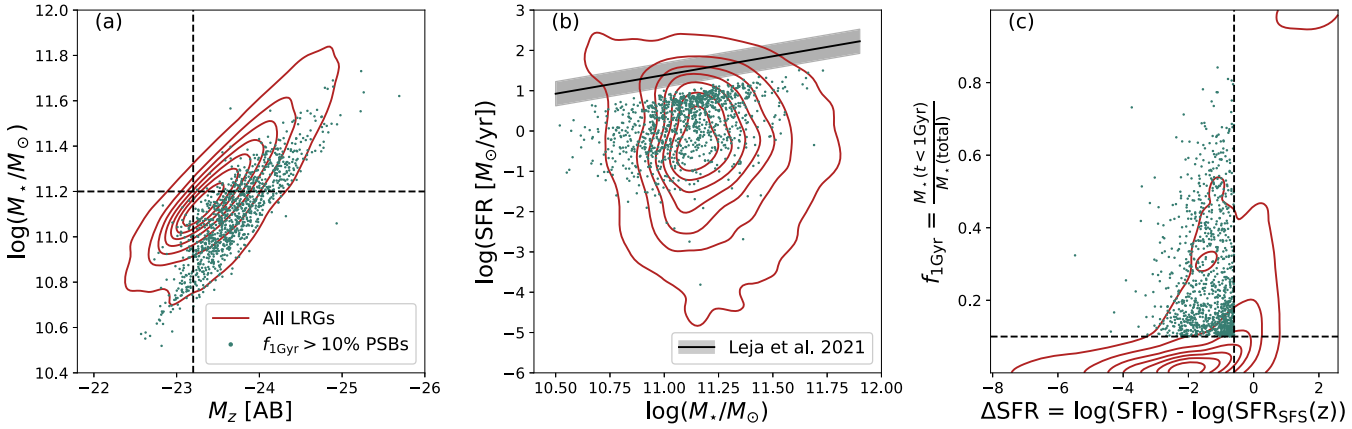

Figure 2. Properties of the full LRG sample (red contours) and a subset of galaxies that recently quenched a significant episode of star formation using our fiducial selection ($f_{1\ \mathrm{Gyr}} > 0.1$, $\Delta\mathrm{SFR} < -0.6$; green points). All plotted points are the median values from the posterior of the `Prospector` fits. In panel (a), we show the stellar mass vs. the absolute magnitude (M_z) along with the magnitude-limited ($M_z < -23.2$) and mass-complete ($\log(M_*/M_\odot > 11.2$) thresholds discussed in Section 2.3. In panel (b), we show the SFR vs. stellar mass, with the star-forming sequence at $z = 0.7$, the median redshift of our sample, shown as a black line with characteristic $\sim$0.3 dex 1σ scatter (Leja et al. 2022). In panel (c), we show the recently quenched selection plane, $f_{1\ \mathrm{Gyr}}$ vs. ΔSFR, with the fiducial selection cuts illustrated as dashed lines. The recently quenched sample is significantly brighter than the parent sample at fixed stellar mass and occupies a unique part of parameter space by having formed a significant amount of recent stellar mass despite being fully quenched.

line cuts (to select against current star formation) and Balmer absorption depth (to select for a stellar population dominated by A-type stars; Dressler & Gunn 1983; Zabludoff et al. 1996; Balogh et al. 1999). Here we leverage the tightly constrained star formation histories to select a physically motivated sample of recently quenched galaxies. First, we focus on selecting a pure quiescent sample. In Figures 2(b) and (c), it is clear that some galaxies that are dusty and star-forming have been selected due to their red colors and exist in the LRG parent sample. To remove these, we perform a conservative cut in ΔSFR, classifying galaxies as quiescent only if their median ΔSFR is $\sim 2\sigma$ (0.6 dex) below the star-forming sequence at their redshift from Leja et al. (2022). This selection, which is highlighted in Figure 2(c), removes 2622 galaxies ($\sim$15% of the total sample). All qualitative results in this work are insensitive to the exact definition of quiescence that we adopt, though exact sample sizes and number densities will, by definition, differ slightly.

Second, we are interested in physically separating the quiescent galaxy population into recent additions to the red sequence and older galaxies. In this work, our definition of recently quenched does not require a burst, as we are interested in classifying all galaxies that rapidly formed a significant amount of stellar mass before quenching as recently quenched galaxies. To select such a sample, we leverage the inferred star formation histories to measure the fraction of the stellar mass formed within the last gigayear ($f_{1\ \mathrm{Gyr}}$) for all galaxies (see also Webb et al. 2020). In combination with the cut for quiescence, selecting galaxies with high $f_{1\ \mathrm{Gyr}}$ identifies a sample that must have rapidly truncated its star formation in order to have formed a large amount of its stellar mass while also reaching quiescence within 1 Gyr. We adopt $f_{1\ \mathrm{Gyr}} > 0.1$ (also shown in Figure 2(c)) for our fiducial recently quenched selection and explore the impact of different thresholds in Section 4. The fiducial selection identifies 1089 recently quenched galaxies from the 15,012 quiescent LRGs using the fiducial $f_{1\ \mathrm{Gyr}} > 0.1$ selection.

This sample of recently quenched galaxies is unparalleled in size beyond $z \gtrsim 1$. In Figure 3, we show the redshift distributions of this sample compared to other large spectroscopic samples of post-starburst galaxies at intermediate redshift. Our sample of hundreds of recently quenched galaxies at $z < 0.8$ is smaller than other samples that select galaxies from the full SDSS (Pattarakijwanich et al. 2016; Suess et al. 2022a) or VIPERS Survey (Rowlands et al. 2018). However, at $z > 1$ (shown in the inset), we find that this sample dramatically increases the number of spectroscopically confirmed recently quenched galaxies at the tail end of cosmic noon.

While our selection of recently quenched galaxies relies on our inferred star formation histories, there are many other selections that use empirical measures of spectroscopic features to select post-starburst galaxies (French 2021). We choose a few common post-starburst identification methods and compare the resulting number densities with our fiducial model (see Section 3.2). For all literature comparisons, we use the same $\Delta\mathrm{SFR} \leqslant -0.6$ criterion for quiescence rather than relying on common empirical metrics like EW H_α, which falls out of our spectral window for most of the sample, or EW [O II], which is an uncertain tracer of SFR due to potential contributions from AGN/LINERs. We note that while exact definitions of H_δ spectral indices vary in the literature (e.g., Alatalo et al. 2016 used H_δ, French et al. 2015 used $\mathrm{H}_{\delta,A}$, and Baron et al. 2022 used $\mathrm{H}_{\delta,F}$), these differences are subtle. We adopt $\mathrm{H}_{\delta,A}$ as our preferred definition, as it is optimized for features from A-type stars (Worthey & Ottaviani 1997). The three selections we compare to our fiducial selection ($f_{1\ \mathrm{Gyr}} > 0.1$ and $\Delta\mathrm{SFR} < -0.6$) are as follows (all numbers quoted are the raw number of galaxies in the full sample, not in a volume-limited sample).

1. $\mathrm{H}_{\delta,A} > 4$ Å. After applying the quiescence criteria, we select 1727 galaxies with $\mathrm{H}_{\delta,A} > 4$ Å following, e.g., French et al. (2015, 2018), Wu et al. (2018), and Yesuf (2022).
2. $\mathrm{H}_{\delta,A} > 5$ Å. We impose a more stringent cut, $\mathrm{H}_{\delta,A} > 5$ Å, following, e.g., Alatalo et al. (2016) and Baron et al. (2022), selecting 1035 post-starburst galaxies.
3. SQuIGG$\vec{L}$E selection. Finally, after applying the quiescence criteria, we use medium-band synthetic rest-frame *UBV* filters to identify post-starburst galaxies with $U - B > 0.975$ and $-0.25 < B - V < 0.45$ following the

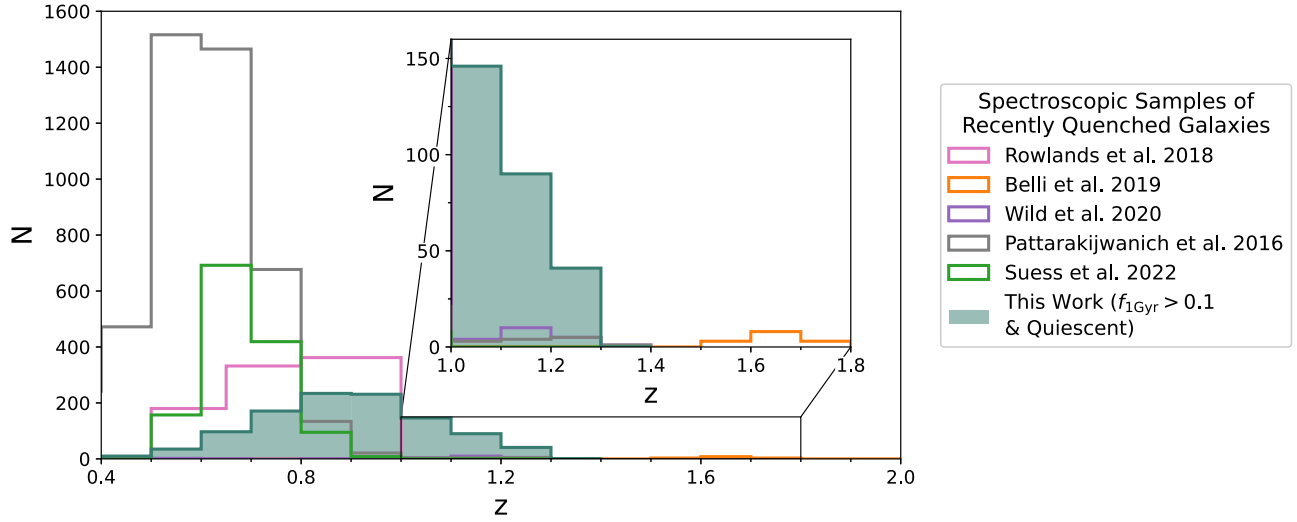

Figure 3. Redshift distributions of spectroscopic samples of recently quenched galaxies in the range $0.4 < z < 2.0$, with an inset focusing on $z > 1$, where the improvement in sample size from this work is most significant. Our fiducial recently quenched sample ($f_{1\ \mathrm{Gyr}} > 0.1$, $\Delta\mathrm{SFR} < -0.6$, selected from the full LRG sample) is shown as a filled green histogram. Other samples shown include PCA-identified post-starburst galaxies from Rowlands et al. (2018) and Wild et al. (2020), galaxies with $t_{50} < 1.5$ Gyr from Belli et al. (2019), galaxies selected with K + A template fitting from the SDSS (Pattarakijwanich et al. 2016), and galaxies selected using rest *UBV* filters from the SQuIGG$\vec{L}$E sample also selected from the SDSS (Suess et al. 2022a).

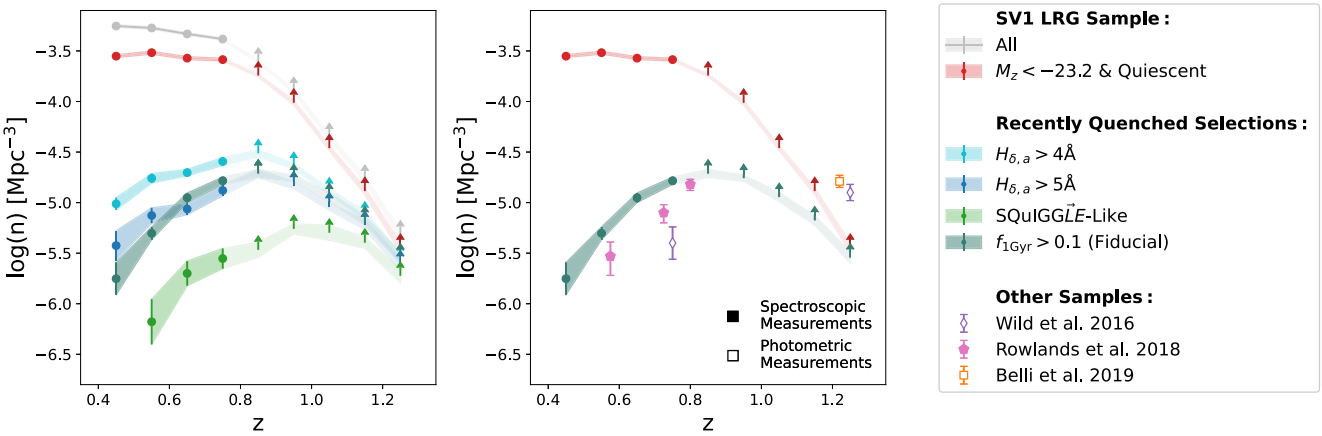

Figure 4. (Left) Number densities within the DESI SV LRG sample (full sample, gray; luminosity-complete and quiescent, red) and a variety of recently quenched selections from the magnitude-limited (see Section 2.3.1) quiescent sample ($H_{\delta,a} > 4$, light blue; $H_{\delta,a} > 5$, dark blue; SQuIGG $\vec{L}$E SED selection, light green; and $f_{1\ \mathrm{Gyr}}$, green). Beyond $z \sim 0.8$, we indicate that the measured number densities are lower limits by plotting them as upward-facing arrows. All recently quenched selections show an increasing number density over the redshift range in which we are complete, with varying normalization resulting from the relative restrictiveness of the post-starburst criteria. (Right) Same magnitude-limited LRG and $f_{1\ \mathrm{Gyr}} > 0.1$ samples as the left panel, in addition to literature measurements (photometric, open symbols; spectroscopic, filled symbols). All three of the Wild et al. (2016; $M_\star > 10^{10.8}\ M_\odot$), Rowlands et al. (2018; $M_\star > 10^{11}\ M_\odot$), and Belli et al. (2019; $M_\star > 10^{10.8}\ M_\odot$) samples show a trend of increasing number density with redshift, but the normalization differs between the different samples as a result of differing stellar mass limits and selection techniques.

procedure for selecting galaxies with SEDs dominated by A-type stellar populations (Suess et al. 2022a). We apply these cuts to the median best-fit models because the spectral coverage is not red enough to consistently overlap with the synthetic *V* filter. This selection finds only 324 post-starburst galaxies.

3.2. The Number Density of Recently Quenched Galaxies

The DESI SV LRG selection is designed to have a uniform comoving number density of galaxies at $0.4 < z < 0.8$, which enables robust determination of the number densities of subsets of the spectroscopic sample (Zhou et al. 2023). For this selection, we use the target density of 1439 deg^{-2} to calculate the number density in bins of $\Delta z = 0.1$ in redshift from $z = 0.4$ to 1.3 by measuring the density of targets for a given selection criterion and dividing by the volume of the bin. We measure the number densities only for the magnitude-limited or mass-complete samples. We utilize jackknife resampling of the 31 SV pointings to calculate the errors on the measured number densities. The errors do not account for catastrophic redshift errors, but those should be very rare ($\leqslant$0.5%; see Zhou et al. 2023) and subdominant relative to cosmic variance and Poisson errors.

The comoving number density of each recently quenched subsample of the magnitude-limited sample as a function of redshift is shown in Figure 4. The raw number density of the DESI LRG SV sample ($z_{\mathrm{fiber}} < 21.6$) is shown in gray. We show the number density of the rest-frame magnitude-limited ($M_z < -23.2$) sample with the fiducial quiescence cut ($\Delta\mathrm{SFR} < -0.6$) in red. We then apply the post-starburst selections outlined in Section 3.1 to the magnitude-limited

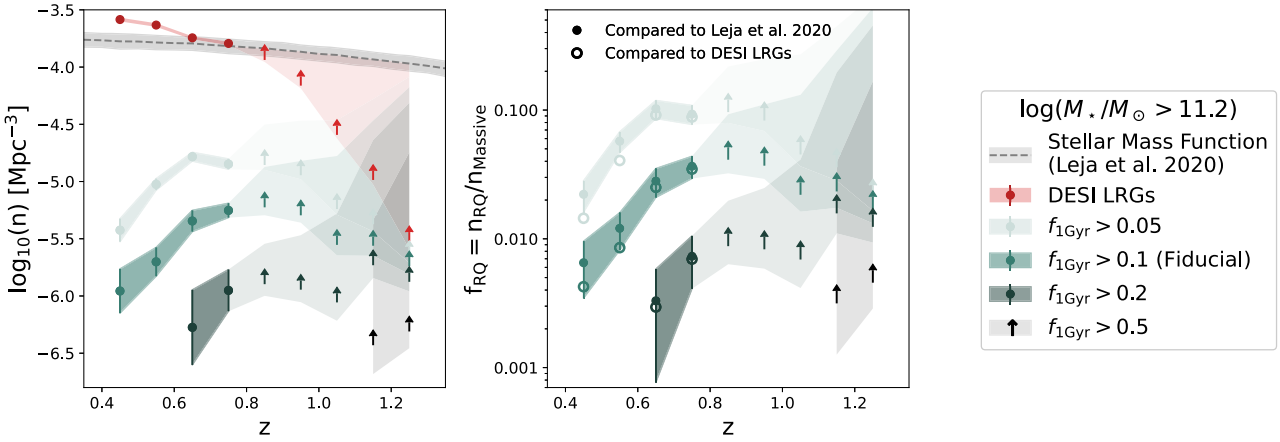

Figure 5. Number densities (left) and fractions (right) of recently quenched galaxies in the mass-complete sample ($\log(M_\star/M_\odot)>11.2$; see Section 2.3.2). The dashed line and gray band (left) represent the stellar mass function of similar-mass galaxies (Leja et al. 2020), and the red points show the number density of all LRGs above the mass limit. The light green, medium green, dark green, and black points represent the number densities and fractions of recently quenched galaxies with $f_{1\,\mathrm{Gyr}}$ greater than 0.05, 0.1, 0.2, and 0.5, respectively, as compared to the stellar mass function from Leja et al. (2020). In the right panel, the open symbols of the same colors show the fraction of recently quenched galaxies compared to our own massive galaxy number density measurements. Above $z = 0.8$, measurements are indicated as lower limits with errors inflated to encapsulate the possibility that all galaxies that were not targeted by DESI meet the selection criterion.

sample. The number densities are shown for $H_{\delta,A} > 4$ Å (light blue), $H_{\delta,A} > 5$ Å (dark blue), SQuIGG$\vec{L}$E-like (light green), and our fiducial $f_{1\,\mathrm{Gyr}} > 0.1$ selection (dark green). In all cases, the number density of post-starburst galaxies rises as a function of redshift in the range of redshifts where the parent LRG sample is complete ($z < 0.8$). Above this, we illustrate that our measurements are lower limits.

In the right panel of Figure 4, we compare our fiducial sample of recently quenched galaxies to several measurements from the literature. We find qualitative agreement with previous studies that observe the number density of recently quenched galaxies increasing with redshift (Wild et al. 2016; Rowlands et al. 2018; Belli et al. 2019). Additionally, the number density of the recently quenched galaxies that we measure is very similar to that of compact star-forming galaxies at $z = 0.5$, adding credence to the argument that such galaxies may be progenitors to local post-starburst galaxies (Tremonti et al. 2007; Diamond-Stanic et al. 2021; Whalen et al. 2022). However, in detail, this comparison is limited by systematic effects; our sample is systematically more massive than other post-starburst samples and is selected using a magnitude (not mass) limit. Additionally, as shown in the left panel of Figure 4, differing identification techniques can significantly impact the measured number density of post-starburst galaxies. Still, a clear consensus emerges from this comparison that recently quenched galaxies were increasingly common at greater look-back times.

3.3. Exploring the Growth of the Red Sequence by Rapidly Quenched Galaxies

In the previous section, we studied the number density of a magnitude-limited sample of recently quenched galaxies to maximize our sample size. Here we attempt to explicitly quantify the fraction of massive galaxies that have recently quenched and joined the red sequence as a function of cosmic time. To do so, we utilize the mass-complete ($\log(M_\star/M_\odot) > 11.2$; see Section 2.3.2) subset of the LRG sample, which we show in the left panel of Figure 5 (red) along with the corresponding stellar mass function from Leja et al. (2020). This measurement overpredicts the stellar mass function by $\sim$0.2 dex at $z \sim 0.4$ while matching well at $z \sim 0.7$. This may be due to systematic differences in the stellar mass estimates (e.g., differences in modeled star formation histories, unmodeled contributions from AGN, or spectro-photometric modeling in our fits versus broadband multi-wavelength SEDs), and the mismatch in redshift evolution may be a result of the targeting incompleteness. As such, we adopt the number densities from the stellar mass function as the total abundance of massive ($\log(M_\star/M_\odot) < 11.2$) galaxies and note that the fractions we measure may be systematically lower than reported by $\sim$0.2 dex. Above $z = 0.8$, where LRG targeting is known to be incomplete, we inflate the upper error bar on the measured lower limits by assuming that every galaxy we have not targeted meets the selection criteria (quantified by the deviation between the measured number density and the stellar mass function) to capture the possibility that every galaxy we did not measure is a recently quenched galaxy. Since this is unlikely due to the lower $M_\star/L$ ratio of recently quenched galaxies, this conservative estimates captures the full range of possibilities in the number density of galaxies in a given selection at $z > 0.8$.

We show the number densities of four different selections of recently quenched galaxies: $f_{1\,\mathrm{Gyr}} > 0.05$ (light green), >0.1 (medium green), >0.2 (dark green), and >0.5 (black). Points that do not appear indicate that the redshift bin contained zero galaxies that met the selection criteria. All four sets of recently quenched galaxies show increasing number densities with redshift. However, even at $z \sim 0.8$, galaxies that formed a large fraction of their stellar mass in the past gigayear are very rare. For example, at $z = 0.8$, galaxies that formed >20% of their stellar mass in the past gigayear were significantly (>1 dex) rarer than those that formed 5% of their stellar mass. We find that the number density of the $f_{1\,\mathrm{Gyr}} > 20\%$ population cannot be decreasing with look-back time; in fact, at $z \sim 1.2$, the lower-limit number density of this population is higher than the number density at $z = 0.8$. The rarity of such objects at intermediate z is extremely consistent with the rarity of "late bloomers," galaxies that formed the majority of their stellar mass in the 2 Gyr before quenching (Dressler et al. 2018). Additionally, we identify a very small population of galaxies that rapidly formed $\geqslant$50% of their stellar mass in the gigayear

before observation at $z = 1.1$–1.3, with lower limits that indicate a number density of at least $\log_{10}(n) > -6.5$ Mpc^{-3}. Similar extreme post-starburst galaxies have been found in photometric samples with comparably low number densities and could represent analogs to the formation of massive quiescent galaxies at high z (Park et al. 2022).

In the right panel of Figure 5, we show the same recently quenched samples as fractions of the total massive galaxy population (shown with filled symbols using the stellar mass function from Leja et al. 2020 as the denominator and open symbols using our own measurements of the LRG number density). We find that galaxies that formed >20% of their stellar mass represent ∼0.5% of the total galaxy population at $z = 0.8$, but by $z \sim 1.2$, they must be at least 1%, with an upper limit that extends to them being ∼50% of the quiescent population. Similarly, the most extreme burst-dominated systems ($f_{1\,\mathrm{Gyr}} > 50\%$) must be at least ∼0.5% of the total galaxy population at $z = 1.2$, but this fraction could be as high as 20%. In contrast, galaxies with $f_{1\,\mathrm{Gyr}} > 5\%$ and >10% are significant even at $z = 0.4$, representing ∼1.5% and 0.5% of the massive galaxy population, and by $z = 0.8$, they are ∼10% and 3% of the total population. Studies of massive quiescent and post-starburst galaxies at similar redshifts have measured similar burst fractions of ∼5% in the bulk of their samples, indicating that at the massive end, the vast majority of "post-starburst" galaxies are the evolutionary products of a recent dusting of star formation, rather than the truncation of their primary epoch of star formation (Patel et al. 2011; French et al. 2018).

The general rarity of extreme massive post-starburst galaxies in this sample is consistent with findings that the formation redshift of $\log(M_\star/M_\odot) = 11.2$ galaxies is $z_{\mathrm{form}} \sim 2$–3 (Gallazzi et al. 2014; Fumagalli et al. 2016; Pacifici et al. 2016; Carnall et al. 2019; Estrada-Carpenter et al. 2019; Díaz-García et al. 2019; Khullar et al. 2022; Webb et al. 2020). At the epochs we are probing, the average massive quiescent galaxy quenched long in the past. However, we find that a significant number of massive galaxies are still quenching with very high $f_{1\,\mathrm{Gyr}}$ well after cosmic noon ($z \sim 2$), and we expect that with a more complete sample at higher redshift, the population dominated by recent star formation would become the norm. The sharp observed decline in rapid quenching after cosmic noon suggests a fundamental shift in the evolutionary histories of massive galaxies. By combining this preliminary analysis with similar stellar population synthesis modeling of larger, mass-complete samples and ancillary data sets (e.g., by analyzing galaxy structural evolution and morphological transformation), we hope to illuminate the physical mechanism(s) that are responsible for halting star formation and sustaining the quiescence of massive galaxies since $z \sim 1$.

4. Discussion and Conclusions

Using the DESI SV sample, we measure nonparametric star formation histories for a novel sample of LRGs. We select physically motivated samples of recently quenched galaxies and leverage the well-characterized parent sample to characterize the increasing number density of recently quenched galaxies with look-back time. We find the following.

1. The sample of quiescent galaxies that formed >10% of their stellar mass in the past gigayear represents a novel spectroscopic sample. The sample of 277 galaxies we identify at $z > 1$ is an order of magnitude larger than previous samples (see Figure 3).
2. The number density of recently quenched galaxies rises steadily with redshift from $z = 0.4$ to 0.8 based on our model selection and empirical identification methods; post-starburst galaxies were more common at earlier cosmic times (see Figure 4).
3. The fraction of massive ($\log(M_\star/M_\odot) > 11.2$) galaxies that have recently quenched their star formation and formed >10% of their stellar mass in the past gigayear rises in this redshift range from $\lesssim$0.5% at $z = 0.4$ to ∼3% at $z = 0.8$ (see Figure 5). Furthermore, at $z > 1$, we find a significant emerging population that formed >20% and >50% of its stellar mass in the past gigayear.

As our criteria for selecting recently quenched galaxies simply required a rapid truncation in a galaxy's SFR that drove a galaxy into quiescence in < 1 Gyr, there is substantial variety in the star formation histories of galaxies that fall into a given selection for $f_{1\,\mathrm{Gyr}}$. The simplicity of this selection allows for simple determination of the rate at which galaxies have entered into quiescence, but it does not distinguish between, for example, a secondary starburst in an already quiescent galaxy and a rapid truncation of the primary epoch of star formation at fixed $f_{1\,\mathrm{Gyr}}$. Future work will endeavor to combine these star formation histories with ancillary data to paint a holistic picture of the quenching of these galaxies. For now, we use constraints on the fraction of galaxies that recently entered into quiescence to discuss possible physical mechanisms that could be driving the rapid cessation of star formation in this sample of galaxies.

One of the most compelling fast processes that could induce, then shut off, star formation and produce post-starburst galaxies is major mergers (e.g., Hopkins et al. 2008). After cosmic noon, simulations have found that many massive galaxies that quench do so via major mergers (e.g., Wellons et al. 2015), which funnel gas inward and induce a burst of star formation that rapidly shuts off. Indeed, many studies of post-starburst galaxies have found that merger features are more common in post-starburst systems (e.g., Pawlik et al. 2016; Sazonova et al. 2021; Ellison et al. 2022; Verrico et al. 2022).

We estimate the relative frequency of major mergers using UNIVERSEMACHINE (Behroozi et al. 2019) and find that 15% and 20% of $\log(M_\star/M_\odot) > 11.2$ galaxies at $z = 0.4$ and 0.8, respectively, experienced a major merger ($M_{\star,2}/M_{\star,1} > 25\%$ in the progenitor galaxies in the merger tree) in the past gigayear. This rate is significantly higher than the 0.5% and 3% fractions we find for our fiducial sample of recently quenched galaxies, and the merger fraction increases more slowly than the recently quenched fraction. Some of this difference may be driven by gas-poor major mergers between already quiescent systems or gas-rich mergers that do not quench, and we conclude that it is plausible that every very massive galaxy that rapidly quenches in the range $0.4 < z < 0.8$ does so as a result of a major merger and that not every major merger results in a post-starburst galaxy. This is in line with predictions from the Illustris TNG simulation that only ∼5% of massive galaxies will quench within ∼500 Myr of coalescence after a major merger (Quai et al. 2021) and indicates that even if major mergers are an essential part of the quenching process, they do not universally produce post-starburst galaxies. However, at high z, our measured lower limits fall short of placing strong constraints.

Still, the high-z tail of our distribution promises to be a very powerful tool for studying rapid quenching. Prior to DESI, only

a small number of spectroscopic continuum observations from surveys could be mined for post-starburst galaxies above $z \gtrsim 1$ (Wild et al. 2020), and often, samples could only be obtained through targeted follow-up of photometrically identified sources (e.g., Belli et al. 2019). Even in the smallest (but highest signal-to-noise ratio) subset of DESI LRG spectra, we have identified an order of magnitude more spectroscopically confirmed recently quenched galaxies than had been measured previously. Future work will leverage these star formation histories further to study trends using parameters such as the time since quenching (Suess et al. 2022a), which has been used in post-starburst populations to constrain the evolution of AGN incidence (Greene et al. 2020), sizes (Setton et al. 2022), molecular gas contents (Bezanson et al. 2022; Spilker et al. 2022), and merger fractions (Verrico et al. 2022). Using the combination of the unique spectroscopically derived moments of the star formation history and ancillary data, we hope to place strong constraints on the mechanisms that drive the quenching of massive galaxies as close to cosmic noon as is currently possible. Future surveys, such as PFS (Greene et al. 2022) and MOONRISE (Maiolino et al. 2020), will extend wavelength coverage into the near-IR, pushing farther in redshift to cosmic noon. In conjunction with this sample, comprehensive studies of the properties of recently quenched galaxies from $z = 0$ to 2 will paint a cohesive picture of the rapid quenching process and its role in producing the present-day quiescent population.

This research is supported by the Director, Office of Science, Office of High Energy Physics of the U.S. Department of Energy under contract No. DE-AC02-05CH11231 and by the National Energy Research Scientific Computing Center, a DOE Office of Science User Facility under the same contract. Additional support for DESI is provided by the U.S. National Science Foundation, Division of Astronomical Sciences under contract No. AST-0950945 to the NSF's National Optical-Infrared Astronomy Research Laboratory; the Science and Technologies Facilities Council of the United Kingdom; the Gordon and Betty Moore Foundation; the Heising-Simons Foundation; the French Alternative Energies and Atomic Energy Commission (CEA); the National Council of Science and Technology of Mexico (CONACYT); the Ministry of Science and Innovation of Spain (MICINN); and the DESI member institutions: https://www.desi.lbl.gov/collaborating-institutions.

D.S. gratefully acknowledges support from NSF-AAG No. 1907697 and the PITT PACC graduate fellowship. The published results were also funded by the Polish National Agency for Academic Exchange (Bekker grant BPN/BEK/2021/1/00298/DEC/1), the European Union's Horizon 2020 research and innovation program under the Maria Skłodowska-Curie (grant agreement No. 754510), and the Spanish Ministry of Science and Innovation through the Juan de la Cierva-formacion program (reference FJC2018-038792-I). D.S. acknowledges helpful conversations with Joel Leja, Wren Suess, Sirio Belli, and Sandro Tacchella that improved this work. We also thank the reviewer for the deep and thorough reading of the paper, resulting in a significantly improved final product.

The authors are honored to be permitted to conduct scientific research on Iolkam Du'ag (Kitt Peak), a mountain with particular significance to the Tohono O'odham Nation. We direct readers to Astrobite's coverage of the Tohono O'odham people and Kitt Peak National Observatory as part of their series on the interactions between predominantly Western astrophysics observatories and Indigenous communities: https://astrobites.org/2019/08/16/a-tale-of-two-observatories.

ORCID iDs

David J. Setton https://orcid.org/0000-0003-4075-7393
Biprateep Dey https://orcid.org/0000-0002-5665-7912
Gourav Khullar https://orcid.org/0000-0002-3475-7648
Rachel Bezanson https://orcid.org/0000-0001-5063-8254
Jeffrey A. Newman https://orcid.org/0000-0001-8684-2222
Jessica N. Aguilar https://orcid.org/0000-0003-0822-452X
Steven Ahlen https://orcid.org/0000-0001-6098-7247
Brett H. Andrews https://orcid.org/0000-0001-8085-5890
David Brooks https://orcid.org/0000-0002-8458-5047
Arjun Dey https://orcid.org/0000-0002-4928-4003
Sarah Eftekharzadeh https://orcid.org/0000-0002-8281-8388
Andreu Font-Ribera https://orcid.org/0000-0002-3033-7312
Satya Gontcho A Gontcho https://orcid.org/0000-0003-3142-233X
Anthony Kremin https://orcid.org/0000-0001-6356-7424
Stephanie Juneau https://orcid.org/0000-0002-0000-2394
Martin Landriau https://orcid.org/0000-0003-1838-8528
Aaron Meisner https://orcid.org/0000-0002-1125-7384
Ramon Miquel https://orcid.org/0000-0002-6610-4836
John Moustakas https://orcid.org/0000-0002-2733-4559
Alan Pearl https://orcid.org/0000-0001-9820-9619
Francisco Prada https://orcid.org/0000-0001-7145-8674
Gregory Tarlé https://orcid.org/0000-0003-1704-0781
Małgorzata Siudek https://orcid.org/0000-0002-2949-2155
Zhimin Zhou https://orcid.org/0000-0002-4135-0977
Hu Zou https://orcid.org/0000-0002-6684-3997

References

Alatalo, K., Lisenfeld, U., Lanz, L., et al. 2016, ApJ, 827, 106
Balogh, M. L., Morris, S. L., Yee, H. K. C., Carlberg, R. G., & Ellingson, E. 1999, ApJ, 527, 54
Baron, D., Netzer, H., Lutz, D., Prochaska, J. X., & Davies, R. I. 2022, MNRAS, 509, 4457
Behroozi, P., Wechsler, R. H., Hearin, A. P., & Conroy, C. 2019, MNRAS, 488, 3143
Belli, S., Newman, A. B., & Ellis, R. S. 2019, ApJ, 874, 17
Bezanson, R., Spilker, J. S., Suess, K. A., et al. 2022, ApJ, 925, 153
Carnall, A. C., McLure, R. J., Dunlop, J. S., et al. 2019, MNRAS, 490, 417
Chabrier, G. 2003, PASP, 115, 763
Choi, J., Dotter, A., Conroy, C., et al. 2016, ApJ, 823, 102
Conroy, C., & Gunn, J. E. 2010, ApJ, 712, 833
Conroy, C., Gunn, J. E., & White, M. 2009, ApJ, 699, 486
Daddi, E., Renzini, A., Pirzkal, N., et al. 2005, ApJ, 626, 680
Dawson, K. S., Kneib, J.-P., Percival, W. J., et al. 2016, AJ, 151, 44
Dawson, K. S., Schlegel, D. J., Ahn, C. P., et al. 2013, AJ, 145, 10
DESI Collaboration, Aghamousa, A., Aguilar, A., et al. 2016a, arXiv:1611.00036
DESI Collaboration, Aghamousa, A., & Aguilar, J. 2016b, arXiv:1611.00037
Dey, A., Schlegel, D. J., Lang, D., et al. 2019, AJ, 157, 168
Diamond-Stanic, A. M., Moustakas, J., Sell, P. H., et al. 2021, ApJ, 912, 11
Díaz-García, L. A., Cenarro, A. J., López-Sanjuan, C., et al. 2019, A&A, 631, A157
Donnari, M., Pillepich, A., Nelson, D., et al. 2019, MNRAS, 485, 4817
Dotter, A. 2016, ApJS, 222, 8
Draine, B. T., Dale, D. A., Bendo, G., et al. 2007, ApJ, 663, 866
Dressler, A., & Gunn, J. E. 1983, ApJ, 270, 7

Dressler, A., Kelson, D. D., & Abramson, L. E. 2018, ApJ, 869, 152
Dressler, A., Kelson, D. D., Abramson, L. E., et al. 2016, ApJ, 833, 251
Dressler, A., Oemler, A., Jr., Poggianti, B. M., et al. 2004, ApJ, 617, 867
Eisenstein, D. J., Annis, J., Gunn, J. E., et al. 2001, AJ, 122, 2267
Ellison, S. L., Wilkinson, S., Woo, J., et al. 2022, MNRAS, 517, L92
Estrada-Carpenter, V., Papovich, C., Momcheva, I., et al. 2019, ApJ, 870, 133
Falcón-Barroso, J., Sánchez-Blázquez, P., Vazdekis, A., et al. 2011, A&A, 532, A95
French, K. D. 2021, PASP, 133, 072001
French, K. D., Yang, Y., Zabludoff, A., et al. 2015, ApJ, 801, 1
French, K. D., Yang, Y., Zabludoff, A. I., & Tremonti, C. A. 2018, ApJ, 862, 2
Fumagalli, M., Franx, M., van Dokkum, P., et al. 2016, ApJ, 822, 1
Gallazzi, A., Bell, E. F., Zibetti, S., Brinchmann, J., & Kelson, D. D. 2014, ApJ, 788, 72
Gallazzi, A., Charlot, S., Brinchmann, J., White, S. D. M., & Tremonti, C. A. 2005, MNRAS, 362, 41
Greene, J., Bezanson, R., Ouchi, M., Silverman, J. & the PFS Galaxy Evolution Working Group 2022, arXiv:2206.14908
Greene, J. E., Setton, D., Bezanson, R., et al. 2020, ApJL, 899, L9
Guy, J., Bailey, S., Kremin, A., et al. 2023, AJ, 165, 144
Hopkins, P. F., Cox, T. J., Kereš, D., & Hernquist, L. 2008, ApJS, 175, 390
Johnson, B., Foreman-Mackey, D., Sick, J., et al. 2021, dfm/python-fsps: python-fsps v0.4.0, Zenodo, doi:10.5281/zenodo.4577191
Johnson, B., & Leja, J. 2017, Bd-J/Prospector: Initial Release, v0.1, Zenodo, doi:10.5281/zenodo.1116491
Juneau, S., Glazebrook, K., Crampton, D., et al. 2005, ApJL, 619, L135
Khullar, G., Bayliss, M. B., Gladders, M. D., et al. 2022, ApJ, 934, 177
Kriek, M., & Conroy, C. 2013, ApJL, 775, L16
Leja, J., Johnson, B. D., Conroy, C., van Dokkum, P. G., & Byler, N. 2017, ApJ, 837, 170
Leja, J., Johnson, B. D., Conroy, C., et al. 2019, ApJ, 877, 140
Leja, J., Speagle, J. S., Johnson, B. D., et al. 2020, ApJ, 893, 111
Leja, J., Speagle, J. S., Ting, Y.-S., et al. 2022, ApJ, 936, 165
Levi, M., Bebek, C., Beers, T., et al. 2013, arXiv:1308.0847
Maiolino, R., Cirasuolo, M., Afonso, J., et al. 2020, Msngr, 180, 24
Maltby, D. T., Almaini, O., Wild, V., et al. 2018, MNRAS, 480, 381
McLure, R. J., Pentericci, L., Cimatti, A., et al. 2018, MNRAS, 479, 25
Muzzin, A., Marchesini, D., Stefanon, M., et al. 2013, ApJ, 777, 18
Pacifici, C., Kassin, S. A., Weiner, B. J., et al. 2016, ApJ, 832, 79
Park, M., Belli, S., Conroy, C., et al. 2022, arXiv:2210.03747
Patel, S. G., Kelson, D. D., Holden, B. P., Franx, M., & Illingworth, G. D. 2011, ApJ, 735, 53
Pattarakijwanich, P., Strauss, M. A., Ho, S., & Ross, N. P. 2016, ApJ, 833, 19
Pawlik, M. M., Wild, V., Walcher, C. J., et al. 2016, MNRAS, 456, 3032
Quai, S., Hani, M. H., Ellison, S. L., Patton, D. R., & Woo, J. 2021, MNRAS, 504, 1888
Rowlands, K., Heckman, T., Wild, V., et al. 2018, MNRAS, 480, 2544
Sánchez-Blázquez, P., Peletier, R. F., Jiménez-Vicente, J., et al. 2006, MNRAS, 371, 703
Sazonova, E., Alatalo, K., Rowlands, K., et al. 2021, ApJ, 919, 134
Schawinski, K., Urry, C. M., Simmons, B. D., et al. 2014, MNRAS, 440, 889
Schlegel, D. J., Finkbeiner, D. P., & Davis, M. 1998, ApJ, 500, 525
Setton, D. J., Verrico, M., Bezanson, R., et al. 2022, ApJ, 931, 51
Silber, J. H., Fagrelius, P., Fanning, K., et al. 2023, AJ, 165, 9
Speagle, J. S. 2020, MNRAS, 493, 3132
Spilker, J. S., Suess, K. A., Setton, D. J., et al. 2022, ApJL, 936, L11
Suess, K. A., Kriek, M., Bezanson, R., et al. 2022a, ApJ, 926, 89
Suess, K. A., Kriek, M., Price, S. H., & Barro, G. 2021, ApJ, 915, 87
Suess, K. A., Leja, J., Johnson, B. D., et al. 2022b, ApJ, 935, 146
Tacchella, S., Conroy, C., Faber, S. M., et al. 2022, ApJ, 926, 134
Tinsley, B. M., & Gunn, J. E. 1976, ApJ, 203, 52
Tremonti, C. A., Moustakas, J., & Diamond-Stanic, A. M. 2007, ApJL, 663, L77
van der Wel, A., Bezanson, R., D'Eugenio, F., et al. 2021, ApJS, 256, 44
Verrico, M., Setton, D. J., Bezanson, R., et al. 2022, arXiv:2211.16532
Weaver, J. R., Davidzon, I., Toft, S., et al. 2022, arXiv:2212.02512
Webb, K., Balogh, M. L., Leja, J., et al. 2020, MNRAS, 498, 5317
Wellons, S., Torrey, P., Ma, C.-P., et al. 2015, MNRAS, 449, 361
Whalen, K. E., Hickox, R. C., Coil, A. L., et al. 2022, AJ, 164, 222
Whitaker, K. E., Kriek, M., van Dokkum, P. G., et al. 2012, ApJ, 745, 179
Wild, V., Almaini, O., Dunlop, J., et al. 2016, MNRAS, 463, 832
Wild, V., Taj Aldeen, L., Carnall, A., et al. 2020, MNRAS, 494, 529
Worthey, G., & Ottaviani, D. L. 1997, ApJS, 111, 377
Wu, P.-F., van der Wel, A., Bezanson, R., et al. 2018, ApJ, 868, 37
Yesuf, H. M. 2022, ApJ, 936, 124
Zabludoff, A. I., Zaritsky, D., Lin, H., et al. 1996, ApJ, 466, 104
Zhou, R., Dey, B., Newman, J. A., et al. 2023, AJ, 165, 58
Zhou, R., Newman, J. A., Dawson, K. S., et al. 2020, RNAAS, 4, 181
Zou, H., Zhou, X., Fan, X., et al. 2017, PASP, 129, 064101